Improved Repetitive Control for High-Precision Satellite Rendezvous

ZHANG Yi, *QI Ruiyun**

College of Automation Engineering, Nanjing University of Aeronautics and Astronautics, Nanjing 211106, P. R. China

(Received 2 September 2021; revised 29 November 2021; accepted 20 December 2021)

Abstract: This paper is focused on control design for high-precision satellite rendezvous systems. A relative motion model of leader-follower satellites described by relative orbit elements (ROE) is adopted, which has clear geometric meaning and high accuracy. An improved repetitive control (IRC) scheme is proposed to achieve high-precision position and velocity tracking, which utilizes the advantage of repetitive control to track the signal precisely and conquers the effects of aperiodic disturbances by adding a nonsingular terminal sliding mode (NSTSM) controller. In addition, the nonlinear state error feedback (NLSEF) is used to improve the dynamic performance of repetitive controller and the radial basis function (RBF) neural networks are employed to approximate the unknown nonlinearities. From rigorous Lyapunov analysis, the stability of the whole closed-loop control system is guaranteed. Finally, numerical simulations are carried out to assess the efficiency and demonstrate the advantages of the proposed control scheme.

Keywords: satellite rendezvous; relative orbit elements; repetitive control; sliding mode control; radial basis function (RBF) neural network

CLC number: TP273 **Document code:** A **Article ID:** 1005-1120(2022)02-0201-18

Nomenclature

Ω/rad	Right ascension of ascending node
ω/rad	Argument of perigee
i/rad	Orbit inclination
a/km	Semi-major axis
e	Eccentricity
θ/rad	True anomaly
u/rad	Argument of attitude
D/(rad•s^{-1})	Relative average drift rate
$\Delta \boldsymbol{e}$	Relative eccentricity vector
$\Delta \boldsymbol{i}$	Relative inclination vector
ΔM/rad	Difference of mean argument of latitude
$\bar{n}$/(rad•s^{-1})	Average angular velocity
n/(rad•s^{-1})	Orbit angular velocity
μ/(m^3•s^{-2})	Earth gravitational constant
r/km	Distance between satellite and the Earth
Δr/km	Distance between two satellites
$\boldsymbol{x}_{\mathrm{p1}}$	Relative position
$\boldsymbol{x}_{\mathrm{p2}}$	Relative velocity
$\boldsymbol{x}_{\mathrm{p1d}}$	Expected relative position
$\boldsymbol{x}_{\mathrm{p2d}}$	Expected relative velocity

0 Introduction

Nowadays, people expect satellites to have longer life spans, for example, refueling a satellite when it runs out of fuel, repairing a satellite when failure happens, or removing components when a satellite assignment is completed. These are called on-orbit services (OOS) for satellites. For these operations, the satellite rendezvous technology is essential.

To gain better satellite rendezvous control performance, an accurate model of satellite formation flying dynamics is essential. Considerable efforts

*Corresponding author, E-mail address: ruiyun.qi@nuaa.edu.cn.

How to cite this article: ZHANG Yi, QI Ruiyun. Improved repetitive control for high-precision satellite rendezvous[J]. Transactions of Nanjing University of Aeronautics and Astronautics, 2022, 39(2): 201-218.

http://dx.doi.org/10.16356/j.1005-1120.2022.02.007

have been devoted to relative motion dynamical equations. One of the most famous and widespread models is Clohessy-Wiltshire (C-W) equations of motion[1], which is used to describe the relative position and velocity between leader and follower satellites in close rendezvous phase[2]. The C-W equations set a rotating Cartesian coordinate system with the origin on the leader satellite, resembling Hill equations in the form[3]. Thus, the equations are also referred to as Hill-Clohessy-Wiltshire (HCW) equations. In order to have a simple and linear expression, the C-W equations make some assumptions, such as the leader satellite orbit being circular, and the Earth being symmetrically sphere. These assumptions not only affect the model precision, but also have effects on fuel consumption.

Among work aiming at promoting the application of C-W equations[4-10], Tschauner-Hempel (T-H) equations[9] describe another widely used model for formation flying, taking the eccentricity of the leader satellite orbit into consideration.

Some work followed another idea to obtain a precise model. A set of six constants can determine an arbitrary satellite orbit, including the orbit shape, position, and satellite motion information. The six constants are named Kepler elements, or absolute orbit elements (AOE) in this paper. Hill[3] mentioned another set of six constants, named relative orbit elements (ROE) in his lunar theory, which determines the relative motion between leader and follower satellites. There is correspondence and association between absolute and relative orbit elements. The relative motion model is established and analyzed based on ROE[11-12]. The ROE has clear geometrical meanings, making the model easy to understand, and the model based on ROE unifies the expression of both elliptical orbit and circular orbit without singularities, which C-W equations and T-H equations fail to do. Most importantly, the model based on ROE is proved to achieve high precision[13]. Despite the abovementioned advantages of ROE, some studies[11-13] focus on trajectory analysis, or only design simple control schemes. Common controllers are usually described in Cartesian coordinates. The rendezvous models described by ROE need transformation before they are suitable for common controllers.

Based on the relative position and relative velocity described by ROE[11-12], our study transfers the relative motion model into the form of Cartesian equations. In this way, the relative motion model in this paper is more suitable for design process control.

Studies have been done on controling a follower satellite to maintain a certain position against a leader satellite. At the early stage, open-loop control schemes were attempted in satellite rendezvous[14-15], which could hardly satisfy the precision and robustness standard of satellite operations. To deal with the outer disturbances and model uncertainties, most methods[16-29] took them as an external unknown term, and designed close-loop control schemes to reduce the impact of the disturbances on the models. Sliding mode control is a popular control scheme in various circumstances[23-29]. In particular, terminal sliding mode (TSM) controller is proved to have finite convergence time and good anti-interference performance[29]. However, the control precision can be further enhanced if the perturbations causing model uncertainties and external disturbances are analyzed separately[15, 23]. As an important indicator in satellite rendezvous mission, tracking precision was not the priority in some studies[24-29], and the precision level achieved by them can be further improved.

Sliding mode control provides stability for tracking. However, in order to meet the precision requirement of satellite rendezvous mission, the control scheme needs modification. Our study combines the advantages of the radial basis function (RBF) of sliding mode control and the repetitive control, consequently improving the precision of the control system, when the stability of the system is guaranteed.

The repetitive controller is commonly seen in high-precision periodic control tasks. The repetitive control loop contains a dynamic model of the track-

ing signal, and the control variable of the last period is added into that of the current period. In time, the repetitive controller is able to track any periodic signals with no steady state error. The impact of the repetitive controller adds up for each period, and a proper control output can remain even when tracking error comes to zero. Hence, the repetitive controller is applied widely in various areas. Nevertheless, there are few examples of satellite rendezvous mission using the repetitive control, because aperiodic disturbances in outer space are amplified by the repetitive controller[30].

Considering model complexity increased by the repetitive controller and the nonlinearity of the control system, the nonlinear state error feedback (NLSEF) containing an extended state observer (ESO) is utilized to estimate the model states and improve the dynamic performance of the repetitive controller. ESO requires very little information and observes well. The error feedback law made by NLSEF is more effective than the linear control law, like traditional PID control. However, it is difficult to analyze the convergence characteristics of NLSEF with ESO. In our study, the repetitive controller improved by NLSEF is regarded as an augmented system, and sliding mode control is used to strengthen the robustness of the system while RBF neural networks are used to estimate model uncertainties.

Compared with the previously work on satellite rendezvous control, the main contributions of this paper are as follows: First, state-space equations of the leader-follower satellites are deduced by using relative position and velocity based on ROE. The model has clear geometric meaning and high accuracy, and most closed-loop control methods can be applied to this model directly. Second, to achieve high-precision satellite rendezvous with external disturbances and model uncertainties, our study takes advantage of the repetitive controller, and tracks expected position and velocity signals accurately. Third, a sliding mode controller is employed to improve the robustness of the repetitive controller, and guarantees that the system is converged in finite time. Further, NLSEF is added to the repetitive controller to adjust the dynamic performance, and the model uncertainties caused by various perturbations are approximated by RBF neural networks.

The remainder of our paper is organized as follows. In Section 1, the dynamic model of leader-follower satellites is proposed. In Section 2, the controller combining the repetitive control and sliding mode control is developed. In Section 3, the stability and convergence property of the control scheme is analyzed strictly. In Section 4, a numeric simulation is presented to verity of the control scheme. Finally, conclusions are drawn in Section 5.

Notations: A specification of symbols is explained in advance.

For an arbitrary vector $\boldsymbol{v}=[v_1 \quad v_2 \quad v_3]^{\mathrm{T}}\in\mathbf{R}^3$ and an arbitrary real constant $c>0$, the exponent of the vector $\boldsymbol{v}^c$ is defined as

$$\boldsymbol{v}^c=\left[\operatorname{sgn}(v_1)|v_1|^c \quad \operatorname{sgn}(v_2)|v_2|^c \quad \operatorname{sgn}(v_3)|v_3|^c\right]^{\mathrm{T}}$$

where for any real number ξ

$$\operatorname{sgn}(\xi)=\begin{cases}1 & \xi>0\\ 0 & \xi=0\\ -1 & \xi<0\end{cases}$$

1 Problem Formulation

In this paper, the leader satellite is in an elliptical orbit, and orbits without any extra control. The control scheme is aimed at the follower satellite.

Our model uses ROE to construct dynamical equations. The model has clear geometrical meanings, unifies the expression of both the elliptical orbit and the circular orbit without singularities, and achieves high precision[14].

1.1 Relative orbit elements

The traditional AOE is the right ascension of ascending node (RAAN) Ω, argument of perigee ω, orbit inclination i, semi-major axis a, the eccentricity of the orbit e, and initial mean anomaly M_0.

Six ROEs are the relative average drift rate D, relative eccentricity vector $\Delta\boldsymbol{e}=[\Delta e_x \quad \Delta e_y]^{\mathrm{T}}$, rela-

tive inclination vector $\Delta \boldsymbol{i}=[\Delta i_x \quad \Delta i_y]^{\mathrm{T}}$, and difference of mean argument of latitude $\Delta M'$[31]. $\Delta \boldsymbol{i}$ describes the orientation of the follower satellite orbit plane. $\Delta \boldsymbol{e}$ describes the shape of the orbit plane. D describes the size of the orbit and $\Delta M'$ describes the position of the orbit.

In Fig.1, O is the center of Earth, P_{l} and P_{f} are perigees of the leader and the follower satellite orbits; B_{l} and B_{f} are ascending nodes of the leader and the follower satellite orbits; $\boldsymbol{e}_{\mathrm{l}}$ and $\boldsymbol{e}_{\mathrm{f}}$ are eccentricity vectors of the leader and the follower satellite the orbits, and $\Delta \boldsymbol{e}$ is relative eccentricity vector; i_{l} and i_{f} are inclination of the leader and the follower satellite orbits; P_{f}' and $\boldsymbol{e}_{\mathrm{f}}'$ are projections of P_{f} and $\boldsymbol{e}_{\mathrm{f}}$ in the leader satellite orbit plane.

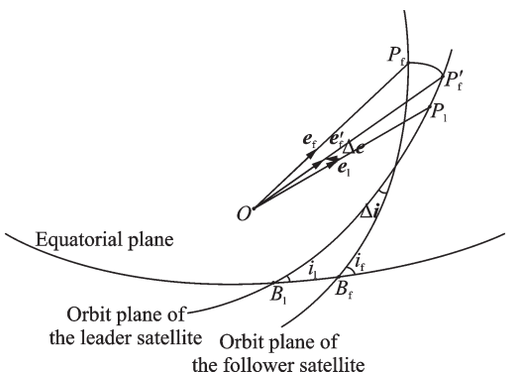

Fig.1 Geometric description of ROE

A strict equivalence relation between AOE and ROE is presented in Ref.[31]. However, in satellite rendezvous situation, two satellites are close to each other. That is $\Delta r/a_{\mathrm{l}} \ll 1$, where Δr is the distance between two satellites, and a_{l} is the semi-major axis of the leader satellite. Then the relationship between ROEs by AOE can be expressed as[31]

$$\begin{cases} D=\bar{n}_{\mathrm{f}}-\bar{n}_{\mathrm{l}} \\ \Delta e_x=e_{\mathrm{f}}\cos\omega_{\mathrm{f}}-e_{\mathrm{l}}\cos\omega_{\mathrm{l}} \\ \Delta e_y=e_{\mathrm{f}}\sin\omega_{\mathrm{f}}-e_{\mathrm{l}}\sin\omega_{\mathrm{l}} \\ \Delta i_x=(\Omega_{\mathrm{f}}-\Omega_{\mathrm{l}})\sin i_{\mathrm{f}} \\ \Delta i_y=i_{\mathrm{l}}-i_{\mathrm{f}} \\ \Delta M'=(\omega_{\mathrm{f}}-\omega_{\mathrm{l}})+(M_{0\mathrm{f}}-M_{0\mathrm{l}})+(\Omega_{\mathrm{f}}-\Omega_{\mathrm{l}})\cos i_{\mathrm{l}} \end{cases} \tag{1}$$

where subscript l represents the leader satellite, and subscript f the follower satellite; $\bar{n}=\sqrt{\mu/a^3}$ is the average angular speed, and μ the Earth gravitational constant.

1.2 Relative dynamical equations

In the local vertical local horizontal (LVLH) frame L-XYZ with the leader satellite centroid as the origin, as shown in Fig.2, where X is along the radial direction of the leader satellite, Y is normal to the orbital plane of the leader satellite, and Z completes the right-handed Cartesian frame.

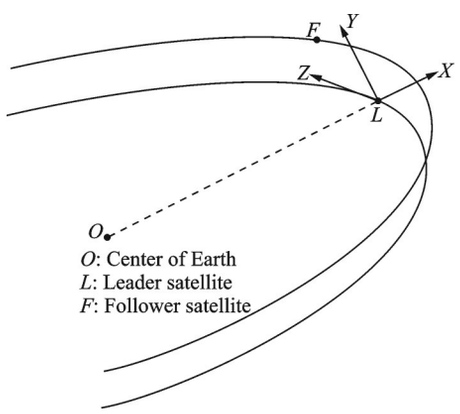

Fig.2 Schematic diagram of LVLH frame

The relative dynamical equations of two close satellites are as follows[31]

$$\begin{cases} x=\left(1+\dfrac{r}{a}\cdot\dfrac{1}{1-e^2}\right)a\left(\Delta e_x\sin u-\Delta e_y\cos u\right)+ \\ \qquad \sqrt{1-e^2}\left(\dfrac{a}{r}\right)a\Delta M'(t)+\Delta_1 \\ y=\left(\dfrac{r}{a}\right)a\left(\Delta i_x\cos u+\Delta i_y\sin u\right) \\ z=a\left(\Delta e_x\cos u+\Delta e_y\sin u\right)+\left(\dfrac{r}{a}\right)a\dfrac{2D}{3\bar{n}}+\Delta_2 \end{cases} \tag{2}$$

where

$$\Delta_1=a\left(\Delta e_y\cos\omega-\Delta e_x\sin\omega\right)\left(\frac{r}{a}\right)\cdot \left[\left(\frac{1-\sqrt{1-e^2}}{e}-e\right)\left(\frac{a}{r}\right)^2-\frac{e}{1-e^2}\right]$$

$$\Delta_2=-\frac{a\sin\theta}{\sqrt{1-e^2}}\left[e\Delta M'+\left(\sqrt{1-e^2}-1\right)\cdot \left(\Delta e_y\cos\omega-\Delta e_x\sin\omega\right)\right]$$

and $r=a(1-e^2)/(1+e\cos\theta)$ is the distance be-

tween the leader satellite and the Earth; $u=\theta+\omega$ is the argument of the latitude of leader satellite; θ is the true anomaly of the leader satellite; Δ_1 is an additional translation term along X direction; and Δ_2 is a pendulum term of Δ_1 on the basis of satellite's elliptical orbit.

Assumption 1[31] Relative average drift rate D and difference of mean argument of latitude $\Delta M'$ are bounded. The first and the second derivatives of D and $\Delta M'$ are bounded.

Remark 1 Since two satellites are close to each other, the differences of their RAANs Ω and orbit inclinations i can be considered small. It is rational to suppose that the differences between their orbit sizes and orbit positions are small, which are described by relative average drift rate D and the difference of mean argument of latitude $\Delta M'$.

Assumption 2[31] Additional terms Δ_1 and Δ_2 are bounded. The first and the second derivatives of the additional terms are bounded.

Remark 2 Except in some special cases where orbit eccentricity e is close to 1, the numerical magnitudes of Δ_1 and Δ_2 are small.

Denote $\sigma_1(t)=\sqrt{1-e^2}\,(a/r)\,a\Delta M'(t)+\Delta_1$ and $\sigma_2(t)=(r/a)\,a(2D/3\bar{n})+\Delta_2$. Based on Assumptions 1 and 2, σ_1, σ_2 and their first and the second derivatives are bounded. Then Eq.(2) turns into

$$\begin{cases} x=\left(1+\dfrac{r}{a}\cdot\dfrac{1}{1-e^2}\right)a\left(\Delta e_x\sin u-\Delta e_y\cos u\right)+\sigma_1 \\ y=\left(\dfrac{r}{a}\right)a\left(\Delta i_x\cos u+\Delta i_y\sin u\right) \\ z=a\left(\Delta e_x\cos u+\Delta e_y\sin u\right)+\sigma_2 \end{cases} \tag{3}$$

The variables with respect to time in Eq.(3) are argument of latitude $u=\theta+\omega$ and distance between the leader satellite and the Earth r. Their derivatives with respect to time are

$$\begin{cases} \dfrac{\mathrm{d}u}{\mathrm{d}t}=\dfrac{\mathrm{d}\theta}{\mathrm{d}t}=\bar{n}\sqrt{1-e^2}\left(\dfrac{a}{r}\right)^2 \\ \dfrac{\mathrm{d}}{\mathrm{d}t}\left(\dfrac{r}{a}\right)=\bar{n}\dfrac{e\sin\theta}{\sqrt{1-e^2}} \\ \dfrac{\mathrm{d}}{\mathrm{d}t}\left(\dfrac{a}{r}\right)=-\bar{n}\left(\dfrac{a}{r}\right)^2\dfrac{e\sin\theta}{\sqrt{1-e^2}} \end{cases}$$

Taking the derivate of Eq.(3) with respect to time leads to

$$\begin{cases} \dfrac{\mathrm{d}x}{\mathrm{d}t}=a\bar{n}\sqrt{1-e^2}\left(\dfrac{a}{r}\right)^2\left(1+\dfrac{r}{a}\cdot\dfrac{1}{1-e^2}\right)\cdot \\ \qquad\left(\Delta e_x\cos u+\Delta e_y\sin u\right)+\dfrac{a\bar{n}}{1-e^2}\cdot \\ \qquad\dfrac{e\sin\theta}{\sqrt{1-e^2}}\left(\Delta e_x\sin u-\Delta e_y\cos u\right)+\dfrac{\mathrm{d}\sigma_1}{\mathrm{d}t} \\ \dfrac{\mathrm{d}y}{\mathrm{d}t}=a\bar{n}\sqrt{1-e^2}\left(\dfrac{a}{r}\right)\left(-\Delta i_x\sin u+\Delta i_y\cos u\right)+ \\ \qquad a\bar{n}\dfrac{e\sin\theta}{\sqrt{1-e^2}}\left(\Delta i_x\cos u+\Delta i_y\sin u\right) \\ \dfrac{\mathrm{d}z}{\mathrm{d}t}=a\bar{n}\sqrt{1-e^2}\left(\dfrac{a}{r}\right)^2\cdot \\ \qquad\left(-\Delta e_x\sin u+\Delta e_y\cos u\right)+\dfrac{\mathrm{d}\sigma_2}{\mathrm{d}t} \end{cases} \tag{4}$$

According to Eqs.(3,4), the state space equations can be obtained as follows

$$\begin{cases} \dfrac{\mathrm{d}^2x}{\mathrm{d}t^2}=-\bar{n}^2\dfrac{(1+e\cos\theta)^5+(1+e\cos\theta)^3}{(1-e^2)^3(2+e\cos\theta)}x- \\ \qquad 2\bar{n}\dfrac{(1+e\cos\theta)^3e\sin\theta}{(1-e^2)^3}z+\dfrac{\mathrm{d}^2\sigma_1}{\mathrm{d}t^2} \\ \dfrac{\mathrm{d}^2y}{\mathrm{d}t^2}=-\bar{n}^2\dfrac{(1+e\cos\theta)^3}{(1-e^2)^3}y \\ \dfrac{\mathrm{d}^2z}{\mathrm{d}t^2}=-\bar{n}^2\dfrac{(1+e\cos\theta)^4}{(1-e^2)^3}z- \\ \qquad 2\bar{n}\dfrac{(1+e\cos\theta)e\sin\theta}{\sqrt{(1-e^2)^3}}\dfrac{\mathrm{d}z}{\mathrm{d}t}+\dfrac{\mathrm{d}^2\sigma_2}{\mathrm{d}t^2} \end{cases} \tag{5}$$

Eq.(5) is a state space expression in Cartesian coordinate system, which is suitable for control design, and the adaptability and high precision of ROE are still preserved.

1.3 Transformation

The true anomaly θ presents the angular distance of a satellite past the point of periapsis measured in degrees, and increases monotonically with time. Then the state variables changing in time can be transformed, and the true anomaly θ is chosen as an independent variable. It is more convenient for the control design process.

Variable x is taken as example[32]. The relationship between the derivative with respect to time $\mathrm{d}x/\mathrm{d}t=\dot{x}$ and the derivative with respect to true anomaly $\mathrm{d}x/\mathrm{d}\theta=x'$ can be expressed as

$$\dot{x}=\frac{\mathrm{d}x}{\mathrm{d}\theta}\frac{\mathrm{d}\theta}{\mathrm{d}t}=nx'$$

$$\ddot{x}=\frac{\mathrm{d}}{\mathrm{d}t}(\dot{x})=\frac{\mathrm{d}}{\mathrm{d}t}(nx')=\frac{\mathrm{d}}{\mathrm{d}\theta}(nx')\frac{\mathrm{d}\theta}{\mathrm{d}t}=(n'x'+nx'')n=nn'x'+n^2x''$$

where n is the orbit angular velocity of the leader satellite, and

$$n=\sqrt{\frac{\mu}{\left(a(1-e^2)\right)^3}}(1+e\cos\theta)^2$$

$$n'=-2\sqrt{\frac{\mu}{\left(a(1-e^2)\right)^3}}(1+e\cos\theta)(e\sin\theta)$$

Then Eq.(5) can be transformed into state space equations with true anomaly θ as independent variable

$$\begin{cases} x''=-\bar{n}^2\dfrac{(1+e\cos\theta)^5+(1+e\cos\theta)^3}{n^2(1-e^2)^3(2+e\cos\theta)}x-\\ \quad 2\bar{n}\dfrac{(1+e\cos\theta)^3e\sin\theta}{n^2(1-e^2)^3}z-\dfrac{n'}{n}x'+\\ \quad nn'\sigma_1'+n^2\sigma_1'' \\ y''=-\bar{n}^2\dfrac{(1+e\cos\theta)^3}{n^2(1-e^2)^3}y-\dfrac{n'}{n}y' \\ z''=-\bar{n}^2\dfrac{(1+e\cos\theta)^4}{n^2(1-e^2)^3}z-\\ \quad \dfrac{n'-2\bar{n}(1+e\cos\theta)e\sin\theta\Big/\sqrt{1-e^2}^3}{n}z'+\\ \quad nn'\sigma_2'+n^2\sigma_2'' \end{cases} \tag{6}$$

Eq.(6) can be rewritten as

$$\begin{bmatrix} x'' \\ y'' \\ z'' \end{bmatrix}=F_1(x,y,z,\theta)+\boldsymbol{\sigma}(\theta) \tag{7}$$

where

$$F_1=\begin{bmatrix} -\bar{n}^2\dfrac{(1+e\cos\theta)^5+(1+e\cos\theta)^3}{n^2(1-e^2)^3(2+e\cos\theta)}x-\dfrac{(1+e\cos\theta)^3e\sin\theta}{n^2(1-e^2)^3}\cdot 2\bar{n}z-\dfrac{n'}{n}x' \\ -\bar{n}^2\dfrac{(1+e\cos\theta)^3}{n^2(1-e^2)^3}y-\dfrac{n'}{n}y' \\ -\dfrac{n'-2\bar{n}(1+e\cos\theta)e\sin\theta\Big/\sqrt{1-e^2}^3}{n}z'-\dfrac{(1+e\cos\theta)^4}{n^2(1-e^2)^3}\cdot\bar{n}^2z \end{bmatrix}$$

and

$$\boldsymbol{\sigma}=\begin{bmatrix} nn'\sigma_1'+n^2\sigma_1'' \\ 0 \\ nn'\sigma_2'+n^2\sigma_2'' \end{bmatrix}$$

As the satellite orbits are in the outer space, they are confronted with various perturbations and disturbances. It is impossible to establish a perfect model. Perturbations lead to measuring errors and modeling inaccuracy, and are presented by $\Delta\boldsymbol{A}(x,y,z,\theta)\in\mathbf{R}^3$. External disturbances are presented by $\boldsymbol{d}_0(\theta)\in\mathbf{R}^3$.

Define $\boldsymbol{x}_{\mathrm{p1}}=\begin{bmatrix} x & y & z \end{bmatrix}^{\mathrm{T}}$ and $\boldsymbol{x}_{\mathrm{p2}}=\begin{bmatrix} v_x & v_y & v_z \end{bmatrix}^{\mathrm{T}}$ as the relative position and relative velocity of the follower satellite, respectively. Based on Eq.(7), the satellite rendezvous model is expressed as

$$\begin{cases} \boldsymbol{x}_{\mathrm{p1}}'=\boldsymbol{x}_{\mathrm{p2}}+\Delta\boldsymbol{A} \\ \boldsymbol{x}_{\mathrm{p2}}'=F_1+\boldsymbol{u}+\boldsymbol{d}(t) \end{cases} \tag{8}$$

where $\boldsymbol{d}=\boldsymbol{d}_0+\boldsymbol{\sigma}\in\mathbf{R}^3$, and $\boldsymbol{u}\in\mathbf{R}^3$ is the control force.

Assumption 3 The unknown disturbances $\boldsymbol{d}$ and the derivatives $\boldsymbol{d}'$ are bounded, i. e. $|d_i|\leqslant\bar{d}_1(i=x,y,z)$ and $|d_i'|\leqslant\bar{d}_2(i=x,y,z)$, where $\bar{d}_1$ and $\bar{d}_2$ are known constants.

1.4 Control objective

In our research, the main difficulties in designing a satellite rendezvous controller are as follows:

(1) Though ROE has specific geometric meaning and high precision, it is necessary to make some assumptions and simplifications to obtain a succinct rendezvous model described by ROE[11-12]. When it is transformed into the Cartesian form, the precision

has to be assured.

(2) After employing the improved repetitive controller, with the existence of ESO, it is difficult to provide the theoretic proof of the stability of the augmented system[31]. Subsequent control schemes are required to handle the increased uncertainties.

(3) The key purpose of our study is to design a control scheme to achieve high-precision satellite rendezvous. Our study outperforms other studies[23-29] with an accuracy level of 5×10^{-4} m.

Based on the relative motion model described in Eq.(8), our study aims at designing an improved repetitive control (IRC) scheme, making relative position $\boldsymbol{x}_{\mathrm{p1}}$ and relative velocity $\boldsymbol{x}_{\mathrm{p2}}$ track given signals $\boldsymbol{x}_{\mathrm{p1d}}=\begin{bmatrix} x_{\mathrm{d}} & y_{\mathrm{d}} & z_{\mathrm{d}} \end{bmatrix}^{\mathrm{T}}$ and $\boldsymbol{x}_{\mathrm{p2d}}=\begin{bmatrix} v_{x\mathrm{d}} & v_{y\mathrm{d}} & v_{z\mathrm{d}} \end{bmatrix}^{\mathrm{T}}$ precisely, even with the existence of model uncertainties and unknown disturbances, and the ultimate thrust the engine can generate is prescribed. The relative position error $\boldsymbol{x}_{\mathrm{p1}}-\boldsymbol{x}_{\mathrm{p1d}}$ is bounded, and the relative speed error $\boldsymbol{x}_{\mathrm{p2}}-\boldsymbol{x}_{\mathrm{p2d}}$ converges to zero in finite time.

2 Control Design

First, as shown in Fig.3, a repetitive controller is designed to track expected position and velocity signals precisely. An NLSEF is used to improve the dynamic performance of the repetitive controller.

Second, as shown in Fig.4, the original rendezvous model and the repetitive controller are regarded as an augmented system. An adaptive sliding mode controller is designed for the augmented system, and ensures the system has good stability and convergence property with disturbances. RBF neural networks are designed to approximate the model uncertainties, and sliding mode surface is designed as nonsingular terminal sliding mode (NSTSM) surface.

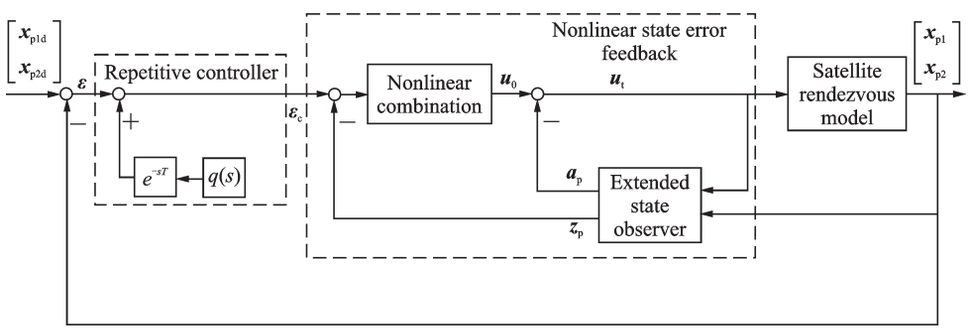

Fig.3 Configuration of repetitive controller

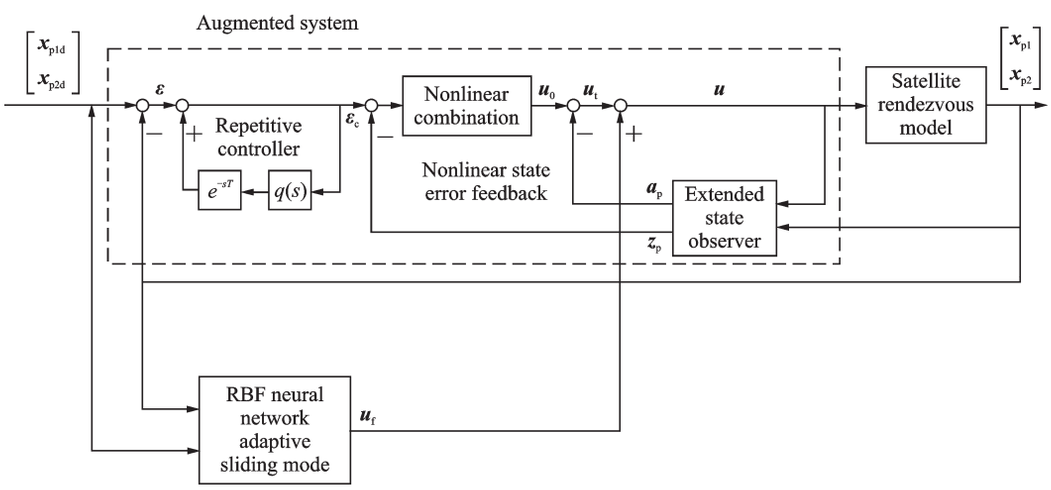

Fig.4 Configuration of repetitive controller and adaptive sliding mode controller

2.1 Repetitive controller

Essentially, the repetitive controller is a high-precision feedback control system, implanting the dynamic model of the external signal in the controller. The repetitive controller can track period signal with no steady state error.

A proper feedback loop can improve the dynamic performance of the repetitive controller.

NLSEF is robust and adaptable, and does not rely on a specific model. This avoids the derivation of the repetitive controller. In NLSEF structure, an extended state observer is utilized to achieve state feedback and model compensation.

As shown in Fig.4, the repetitive controller includes a delay element e^{-sT} and dynamic model of the external signal $q(s)$, where T is the delay constant. $\boldsymbol{\varepsilon}_c \in \mathbf{R}^6$ is the output of the repetitive controller, and $\boldsymbol{u}_t \in \mathbf{R}^3$ is the output of the repetitive controller with NLSEF.

According to Lemma 1 in Ref.[33] (see the Appendix), to track the states of the rendezvous model controlled by the repetitive controller, the observer in NLSEF is designed as

$$\begin{cases} \dot{\boldsymbol{z}}_1 = \boldsymbol{z}_2 - g_1(\boldsymbol{z}_1 - \boldsymbol{x}_{p1}) \\ \dot{\boldsymbol{z}}_2 = \boldsymbol{z}_3 - g_2(\boldsymbol{z}_1 - \boldsymbol{x}_{p1}) + \boldsymbol{u}_t \\ \dot{\boldsymbol{z}}_3 = -g_3(\boldsymbol{z}_1 - \boldsymbol{x}_{p1}) \end{cases} \tag{9}$$

where $\boldsymbol{z}_1 \in \mathbf{R}^3$, $\boldsymbol{z}_2 \in \mathbf{R}^3$ and $\boldsymbol{z}_3 \in \mathbf{R}^3$ are state variables of the observer. The functions $g_1(\cdot)$, $g_2(\cdot)$ and $g_3(\cdot)$ in Eq.(9) are chosen as[31]

$$g_1(\boldsymbol{z}_1 - \boldsymbol{x}_{p1}) = b_{01}\,\mathrm{fal}(\boldsymbol{z}_1 - \boldsymbol{x}_{p1}, \alpha_1, \delta_1)$$
$$g_2(\boldsymbol{z}_1 - \boldsymbol{x}_{p1}) = b_{02}\,\mathrm{fal}(\boldsymbol{z}_1 - \boldsymbol{x}_{p1}, \alpha_1, \delta_1)$$
$$g_3(\boldsymbol{z}_1 - \boldsymbol{x}_{p1}) = b_{03}\,\mathrm{fal}(\boldsymbol{z}_1 - \boldsymbol{x}_{p1}, \alpha_1, \delta_1)$$

where $b_{0i}(i = 1, 2, 3)$, α_1 and δ_1 are adjustable parameters, and function

$$\mathrm{fal}(\boldsymbol{\varepsilon}, \alpha, \delta) = \begin{cases} |\boldsymbol{\varepsilon}|^{\alpha}\,\mathrm{sgn}(\boldsymbol{\varepsilon}) & \|\boldsymbol{\varepsilon}\| > \delta \\ \boldsymbol{\varepsilon}/\delta^{1-\alpha} & \|\boldsymbol{\varepsilon}\| \leqslant \delta \end{cases}$$

Especially, denote $\boldsymbol{a}_p = \boldsymbol{z}_3 \in \mathbf{R}^3$, which compensates the unknown part of the model, and denote $\boldsymbol{z}_p = [\boldsymbol{z}_1^{\mathrm{T}} \quad \boldsymbol{z}_2^{\mathrm{T}}]^{\mathrm{T}} \in \mathbf{R}^6$, which tracks the state variables of the model controlled by the repetitive controller.

Denote the output of the repetitive controller $\boldsymbol{\varepsilon}_c = [\boldsymbol{\varepsilon}_{c1}^{\mathrm{T}} \quad \boldsymbol{\varepsilon}_{c2}^{\mathrm{T}}]^{\mathrm{T}}$, where $\boldsymbol{\varepsilon}_{c1} \in \mathbf{R}^3$ and $\boldsymbol{\varepsilon}_{c2} \in \mathbf{R}^3$. The NLSEF control law $\boldsymbol{u}_0 \in \mathbf{R}^3$ is expressed as

$$u_{0i} = b_1\,\mathrm{fal}(\boldsymbol{\varepsilon}_{c1i}, \alpha, \delta) + b_2\,\mathrm{fal}(\boldsymbol{\varepsilon}_{c2i}, \alpha, \delta)$$
$$i = x, y, z \tag{10}$$

where b_1, b_2, α and δ are adjustable parameters.

The satellite rendezvous model and the repetitive controller with NLSEF are regarded as an augmented system. Based on the rendezvous model described in Eq.(8), observer described in Eq.(9), and control law described in Eq.(10), the augmented system can be described as

$$\begin{cases} \boldsymbol{x}_{p1}' = \boldsymbol{x}_{p2} + \Delta \boldsymbol{A} \\ \boldsymbol{x}_{p2}' = \boldsymbol{F}_2(\boldsymbol{x}_{p1}, \boldsymbol{x}_{p2}, \boldsymbol{z}_1, \boldsymbol{\varepsilon}_c, \theta) + \boldsymbol{u} + \boldsymbol{d} \end{cases} \tag{11}$$

where $\boldsymbol{F}_2 = \boldsymbol{F}_1 + \boldsymbol{u}_0 - \boldsymbol{a}_p$.

Although the augmented system described in Eq.(11) is able to track expected relative position and velocity precisely without additional control force $\boldsymbol{u}$, it is poor at dealing with unknown disturbances. An adaptive sliding mode controller is designed to address this problem.

2.2 Sliding mode controller

Sliding mode control belongs to variable structure control. The design process is independent from system structure and external disturbances, which makes the sliding mode controller robust.

RBF neural networks are feedforward networks. Theoretically, the output of the neural networks can approximate any function with any accuracy. The networks can be divided into three parts: Input layer, hidden layer, and output layer.

The hidden layer contains some nodes, which are also known as neural cells. The number of hidden layer nodes are N. $\boldsymbol{h} = [\boldsymbol{h}_x \quad \boldsymbol{h}_y \quad \boldsymbol{h}_z] \in \mathbf{R}^{N \times 3}$ is the RBF. Variable x is taken as an example. The output of the jth neural node is chosen as a Gaussian function

$$h_{xj} = \exp\left(\frac{\|x - \boldsymbol{c}_{xj}\|^2}{2b_{xj}^2}\right)$$

and $\boldsymbol{h}_x = [h_{x1} \quad h_{x2} \quad \cdots \quad h_{xj} \quad \cdots \quad h_{xN}]^{\mathrm{T}} \in \mathbf{R}^N$, where $j = 1, 2, \cdots, N$ presents the serial number of the node; $\boldsymbol{c}_{xj}$ is the central vector of each node, and b_{xj}

is the breadth of Gaussian function of each node.

The ideal output is

$$\Delta \boldsymbol{A}=\begin{bmatrix}\boldsymbol{W}_x^{*\mathrm{T}}\boldsymbol{h}_x(x)\\ \boldsymbol{W}_y^{*\mathrm{T}}\boldsymbol{h}_y(y)\\ \boldsymbol{W}_z^{*\mathrm{T}}\boldsymbol{h}_z(z)\end{bmatrix}+\begin{bmatrix}\varepsilon_{x\mathrm{n}}\\ \varepsilon_{y\mathrm{n}}\\ \varepsilon_{z\mathrm{n}}\end{bmatrix} \tag{12}$$

where $\boldsymbol{W}_i^*\in\mathrm{R}^N(i=x,y,z)$ are the ideal weights, and $\varepsilon_{in}(i=x,y,z)$ are bonded approximate errors, i.e. $|\varepsilon_{in}|\leqslant\bar{\varepsilon}_{\mathrm{n}}(i=x,y,z)$, where $\bar{\varepsilon}_{\mathrm{n}}$ is a constant[34].

The estimated output is

$$\Delta\hat{\boldsymbol{A}}=\begin{bmatrix}\hat{\boldsymbol{W}}_x^{\mathrm{T}}\boldsymbol{h}_x(x)\\ \hat{\boldsymbol{W}}_y^{\mathrm{T}}\boldsymbol{h}_y(y)\\ \hat{\boldsymbol{W}}_z^{\mathrm{T}}\boldsymbol{h}_z(z)\end{bmatrix} \tag{13}$$

where $\hat{\boldsymbol{W}}_i\in\mathrm{R}^N(i=x,y,z)$ are estimated weights. The estimated weight vector is defined as $\hat{\boldsymbol{W}}=\begin{bmatrix}\hat{\boldsymbol{W}}_x & \hat{\boldsymbol{W}}_y & \hat{\boldsymbol{W}}_z\end{bmatrix}\in\mathrm{R}^{N\times 3}$.

The estimated weight errors of each axis $\tilde{\boldsymbol{W}}_i\in\mathrm{R}^N(i=x,y,z)$ are

$$\tilde{\boldsymbol{W}}_i=\hat{\boldsymbol{W}}_i-\boldsymbol{W}_i^* \tag{14}$$

and the estimated weight error vector is defined as $\tilde{\boldsymbol{W}}=\begin{bmatrix}\tilde{\boldsymbol{W}}_x & \tilde{\boldsymbol{W}}_y & \tilde{\boldsymbol{W}}_z\end{bmatrix}\in\mathrm{R}^{N\times 3}$.

A backstepping algorithm[35] is used to design the sliding mode control law. The backstepping algorithm is divided into two steps.

Step 1 Define the relative position error as $\boldsymbol{\delta}_1=\boldsymbol{x}_{\mathrm{p1}}-\boldsymbol{x}_{\mathrm{1d}}\in\mathrm{R}^3$. Taking derivative of $\boldsymbol{\delta}_1$ leads to

$$\boldsymbol{\delta}_1'=\boldsymbol{x}_{\mathrm{p1}}'-\boldsymbol{x}_{\mathrm{1d}}' \tag{15}$$

The estimated weights $\hat{\boldsymbol{W}}_i(i=x,y,z)$ are updated by

$$\hat{\boldsymbol{W}}_i'=\Gamma_i\delta_{1i}\boldsymbol{h}_i-\sigma_i\hat{\boldsymbol{W}}_i \tag{16}$$

where Γ_i and σ_i are adjustable parameters.

Define the virtual control variable as $\boldsymbol{r}_{\mathrm{2d}}\in\mathrm{R}^3$ and design the virtual control as

$$\boldsymbol{r}_{\mathrm{2d}}=-\boldsymbol{k}\boldsymbol{\delta}_1-\hat{\boldsymbol{W}}^{\mathrm{T}}\boldsymbol{h}+\boldsymbol{x}_{\mathrm{p1d}}' \tag{17}$$

where $\boldsymbol{k}=\mathrm{diag}(k_x,k_y,k_z)\in\mathrm{R}^{3\times 3}$ is an adjustable parameter.

Step 2 Define relative speed error as $\boldsymbol{\delta}_2=\boldsymbol{x}_{\mathrm{p2}}-\boldsymbol{r}_{\mathrm{2d}}\in\mathrm{R}^3$. Taking derivative of $\boldsymbol{\delta}_2$ leads to

$$\boldsymbol{\delta}_2'=\boldsymbol{x}_{\mathrm{p2}}'-\boldsymbol{r}_{\mathrm{2d}}' \tag{18}$$

Usually, the sliding mode surface is designed linear. To obtain a more robust performance, and make the satellite come and stay at the designated position in limited time, this paper employs NSTSM surface $\boldsymbol{s}\in\mathrm{R}^3$ as[34]

$$\boldsymbol{s}=\boldsymbol{\delta}_2+\beta\boldsymbol{\delta}_2'^{\gamma} \tag{19}$$

where β and γ are adjustable parameters, and γ is a quotient of two odd numbers, satisfying $1<\gamma<2$.

The sliding mode control variable $\boldsymbol{u}_{\mathrm{f}}\in\mathrm{R}^3$ is designed as

$$\boldsymbol{u}_{\mathrm{f}}=\boldsymbol{u}_{\mathrm{f1}}+\boldsymbol{u}_{\mathrm{f2}} \tag{20}$$

where

$$\boldsymbol{u}_{\mathrm{f1}}=-F_2+\boldsymbol{r}_{\mathrm{2d}}'$$

$$\boldsymbol{u}_{\mathrm{f2}}=-\int_0^{\theta}\left[(1/\gamma)(1/\beta)\cdot\boldsymbol{\delta}_2'^{\,2-\gamma}+p_1\,\mathrm{sgn}(\boldsymbol{s})+p_2\boldsymbol{s}\right]\mathrm{d}\tau$$

where p_1 and p_2 are adjustable parameters.

3 Analysis of Convergence and Boundedness

The satellite rendezvous model described in Eq.(8) is established in Section 1. In Section 2.1, the model is augmented by a repetitive controller with NLSEF to gain precise tracking ability, described in Eq.(11). And in Section 2.2, an adaptive sliding mode controller is used to assure the stability and robustness of the augmented system with unknown disturbances and model uncertainties.

This section uses Lyapunov-like composite energy functions (CEF) to analyze the convergence and boundedness of the system[36].

Theorem 1 Based on Assumptions 1, 2 and 3, for dynamic system described in Eq.(11), the adaptive law is designed as Eq.(16), the NSTSM surface is employed as Eq.(19), and the controller is adopted as Eq.(20), then relative position error $\boldsymbol{\delta}_1$ is bounded, the relative speed error $\boldsymbol{\delta}_2$ converges to zero in finite time, and the relative stations of follower satellite $\boldsymbol{x}_{\mathrm{p1}}$ and $\boldsymbol{x}_{\mathrm{p2}}$ are able to converge to designate rendezvous states.

Proof

(1) Convergence of relative speed error $\boldsymbol{\delta}_2$

Define a Lyapunov function as

$$V_1=\frac{1}{2}\boldsymbol{s}^{\mathrm{T}}\boldsymbol{s} \tag{21}$$

Taking derivative with respect to the true anomaly θ of Eq.(21) leads to

$$V_1' = \boldsymbol{s}^{\mathrm{T}}\boldsymbol{s}' \tag{22}$$

Taking derivation of Eq.(19) leads to

$$\boldsymbol{s}' = \boldsymbol{\delta}_2' + \beta\gamma(\boldsymbol{\delta}_2'^{\mathrm{T}})^{(\gamma-1)}\boldsymbol{\delta}_2'' \tag{23}$$

According to Eq.(23), Eq.(22) is written as

$$V_1' = \boldsymbol{s}^{\mathrm{T}}\left(\boldsymbol{\delta}_2' + \beta\gamma(\boldsymbol{\delta}_2'^{\mathrm{T}})^{(\gamma-1)}\boldsymbol{\delta}_2''\right) \tag{24}$$

According to Eqs.(18,10,20), we have

$$\begin{aligned}\boldsymbol{\delta}_2' &= \boldsymbol{x}_{\mathrm{p2}}' - \boldsymbol{r}_{\mathrm{2d}}' = \\ &\boldsymbol{F}_2 + \boldsymbol{u}_{\mathrm{f}} + \boldsymbol{d} - \boldsymbol{r}_{\mathrm{2d}}' = \\ &\boldsymbol{F}_2 + \boldsymbol{u}_{\mathrm{f1}} + \boldsymbol{u}_{\mathrm{f2}} + \boldsymbol{d} - \boldsymbol{r}_{\mathrm{2d}}' = \\ &\boldsymbol{u}_{\mathrm{f2}} + \boldsymbol{d}\end{aligned} \tag{25}$$

Taking derivative of Eq.(25) leads to

$$\boldsymbol{\delta}_2'' = \boldsymbol{u}_{\mathrm{f2}}' + \boldsymbol{d}' \tag{26}$$

Substituting Eqs.(26,20) into Eq.(24) leads to

$$\begin{aligned}V_1' = &\boldsymbol{s}^{\mathrm{T}}\left[\boldsymbol{\delta}_2' + \beta\gamma(\boldsymbol{\delta}_2'^{\mathrm{T}})^{(\gamma-1)}(\boldsymbol{u}_{\mathrm{f2}}' + \boldsymbol{d}')\right] = \\ &\boldsymbol{s}^{\mathrm{T}}\left[\boldsymbol{\delta}_2' + \beta\gamma(\boldsymbol{\delta}_2'^{\mathrm{T}})^{(\gamma-1)}\cdot\right. \\ &\left.\left(-\frac{1}{\gamma}\cdot\frac{1}{\beta}\cdot\boldsymbol{\delta}_2'^{(2-\gamma)} - p_1\,\mathrm{sgn}(\boldsymbol{s}) - p_2\boldsymbol{s} + \boldsymbol{d}'\right)\right] = \\ &\boldsymbol{s}^{\mathrm{T}}\boldsymbol{\delta}_2' + \beta\gamma\boldsymbol{s}^{\mathrm{T}}(\boldsymbol{\delta}_2'^{\mathrm{T}})^{(\gamma-1)}\cdot \\ &\left(-\frac{1}{\gamma}\cdot\frac{1}{\beta}\cdot\boldsymbol{\delta}_2'^{(2-\gamma)} - p_1\,\mathrm{sgn}(\boldsymbol{s}) - p_2\boldsymbol{s} + \boldsymbol{d}'\right)\end{aligned} \tag{27}$$

Expand Eq.(27) into the form of addition of triaxial components

$$\begin{aligned}V_1' = &\boldsymbol{s}^{\mathrm{T}}\left[\boldsymbol{\delta}_2' + \beta\gamma(\boldsymbol{\delta}_2'^{\mathrm{T}})^{(\gamma-1)}(\boldsymbol{u}_{\mathrm{f2}}' + \boldsymbol{d}')\right] = \\ &\boldsymbol{s}^{\mathrm{T}}\left[\boldsymbol{\delta}_2' + \beta\gamma(\boldsymbol{\delta}_2'^{\mathrm{T}})^{(\gamma-1)}\cdot\right. \\ &\left.\left(-\frac{1}{\gamma}\cdot\frac{1}{\beta}\cdot\boldsymbol{\delta}_2'^{(2-\gamma)} - p_1\,\mathrm{sgn}(\boldsymbol{s}) - p_2\boldsymbol{s} + \boldsymbol{d}'\right)\right] = \\ &\boldsymbol{s}^{\mathrm{T}}\boldsymbol{\delta}_2' + \beta\gamma\boldsymbol{s}^{\mathrm{T}}(\boldsymbol{\delta}_2'^{\mathrm{T}})^{(\gamma-1)}\cdot \\ &\left(-\frac{1}{\gamma}\cdot\frac{1}{\beta}\cdot\boldsymbol{\delta}_2'^{(2-\gamma)} - p_1\,\mathrm{sgn}(\boldsymbol{s}) - p_2\boldsymbol{s} + \boldsymbol{d}'\right)\end{aligned} \tag{28}$$

Based on Assumption 3 that $|d_i'| \leqslant \bar{d}_2 (i = x, y, z)$, it is possible to design a positive control law parameter p_2, and get

$$\begin{aligned}&V_1' \leqslant \sum_{i=x}^{z}\beta\gamma\delta_{2i}'^{(\gamma-1)}\left(-p_1|s_i| + |d_i'||s_i|\right) \leqslant \\ &\sum_{i=x}^{z}\beta\gamma\delta_{2i}'^{(\gamma-1)}\left(-p_1|s_i| + \bar{d}_2|s_i|\right)\end{aligned}$$

According to the limitation of the parameters that $\beta > 0$ and $1 < \gamma < 2$, then $\beta\gamma\boldsymbol{\delta}_2'^{(\gamma-1)} \geqslant \boldsymbol{0}$. If parameter $p_1 > \bar{d}_2$ and $\boldsymbol{s} \neq \boldsymbol{0}$, then $V_1' \leqslant 0$ is promised, and equality only holds when $\boldsymbol{\delta}_2' = \boldsymbol{0}$. The specific situation when $\boldsymbol{\delta}_2' = \boldsymbol{0}$ and $\boldsymbol{s} \neq \boldsymbol{0}$ is discussed below.

Taking derivative of Eq.(18) leads to

$$\boldsymbol{\delta}_2'' = \boldsymbol{x}_{\mathrm{p2}}'' - \boldsymbol{r}_{\mathrm{2d}}'' \tag{29}$$

Substituting Eqs.(10,20) into Eq.(29) leads to

$$\begin{aligned}&\boldsymbol{\delta}_2'' = \boldsymbol{F}_2' + \boldsymbol{u}_{\mathrm{f}}' + \boldsymbol{d}' - \boldsymbol{r}_{\mathrm{2d}}'' = \\ &\boldsymbol{F}_2' - \boldsymbol{F}_2' + \boldsymbol{r}_{\mathrm{2d}}'' - \frac{1}{\gamma}\cdot\frac{1}{\beta}\cdot\boldsymbol{\delta}_2'^{(2-\gamma)} - \\ &p_1\,\mathrm{sgn}(\boldsymbol{s}) - p_2\boldsymbol{s} + \boldsymbol{d}' - \boldsymbol{r}_{\mathrm{2d}}'' = \\ &-\frac{1}{\gamma}\cdot\frac{1}{\beta}\cdot\boldsymbol{\delta}_2'^{(2-\gamma)} - p_1\,\mathrm{sgn}(\boldsymbol{s}) - p_2\boldsymbol{s} + \boldsymbol{d}'\end{aligned} \tag{30}$$

Since $\boldsymbol{\delta}_2' = \boldsymbol{0}$ and $p_1 > \bar{d}_2$, Eq.(30) turns into

$$\boldsymbol{\delta}_2'' = -p_1\,\mathrm{sgn}(\boldsymbol{s}) - p_2\boldsymbol{s} + \boldsymbol{d}'$$

It can be observed that when $\boldsymbol{s} > \boldsymbol{0}$, $\boldsymbol{\delta}_2'' < \boldsymbol{0}$, $\boldsymbol{\delta}_2'$ decreases; when $\boldsymbol{s} < \boldsymbol{0}$, $\boldsymbol{\delta}_2'' > \boldsymbol{0}$, $\boldsymbol{\delta}_2'$ increases. That means $\boldsymbol{\delta}_2' = \boldsymbol{0}$ and $\boldsymbol{\delta}_2 \neq \boldsymbol{0}$ is not a stable state, so is the state $V_1' = 0$. Therefore, the system states will tend towards sliding mode surface $\boldsymbol{s} = 0$ and the relative speed error $\boldsymbol{\delta}_2$ will converge as well[37].

(2) Boundedness of relative position error $\boldsymbol{\delta}_1$ and estimated weight error vector $\tilde{\boldsymbol{W}}$

Define a Lyapunov function as

$$V_2 = \frac{1}{2}\boldsymbol{\delta}_1^{\mathrm{T}}\boldsymbol{\delta}_1 + \sum_{i=x}^{z}\frac{1}{2}\tilde{\boldsymbol{W}}_i^{\mathrm{T}}\Gamma_i^{-1}\tilde{\boldsymbol{W}}_i \tag{31}$$

Taking derivative of Eq.(31) leads to

$$V_2' = \boldsymbol{\delta}_1^{\mathrm{T}}\boldsymbol{\delta}_1' + \sum_{i=x}^{z}\Gamma_i^{-1}\tilde{\boldsymbol{W}}_i^{\mathrm{T}}\hat{\boldsymbol{W}}_i' \tag{32}$$

Substituting Eqs.(15,10) into Eq.(32) leads to

$$\begin{aligned}V_2' = &\boldsymbol{\delta}_1^{\mathrm{T}}\left(\boldsymbol{x}_{\mathrm{p1}}' - \boldsymbol{x}_{\mathrm{p1d}}'\right) + \sum_{i=x}^{z}\Gamma_i^{-1}\tilde{\boldsymbol{W}}_i^{\mathrm{T}}\hat{\boldsymbol{W}}_i' = \\ &\boldsymbol{\delta}_1^{\mathrm{T}}\left(\boldsymbol{x}_{\mathrm{p2}} + \Delta\boldsymbol{A} - \boldsymbol{x}_{\mathrm{p1d}}'\right) + \sum_{i=x}^{z}\Gamma_i^{-1}\tilde{\boldsymbol{W}}_i^{\mathrm{T}}\hat{\boldsymbol{W}}_i'\end{aligned} \tag{33}$$

According to Eq.(12), Eq.(33) turns into

$$\begin{aligned}V_2' = &\boldsymbol{\delta}_1^{\mathrm{T}}\left(\boldsymbol{x}_{\mathrm{p2}} + \boldsymbol{W}^{*\mathrm{T}}\boldsymbol{h} + \boldsymbol{\varepsilon}_{\mathrm{n}} - \boldsymbol{x}_{\mathrm{p1d}}'\right) + \\ &\sum_{i=x}^{z}\Gamma_i^{-1}\tilde{\boldsymbol{W}}_i^{\mathrm{T}}\hat{\boldsymbol{W}}_i' = \\ &\boldsymbol{\delta}_1^{\mathrm{T}}\left(\boldsymbol{\delta}_2 + \boldsymbol{r}_{\mathrm{2d}} + \boldsymbol{W}^{*\mathrm{T}}\boldsymbol{h} + \boldsymbol{\varepsilon}_{\mathrm{n}} - \boldsymbol{x}_{\mathrm{p1d}}'\right) + \\ &\sum_{i=x}^{z}\Gamma_i^{-1}\tilde{\boldsymbol{W}}_i^{\mathrm{T}}\hat{\boldsymbol{W}}_i'\end{aligned} \tag{34}$$

Substituting Eqs.(17,14) into Eq.(34) leads to

$$V_2'=\boldsymbol{\delta}_1^{\mathrm{T}}\left(\boldsymbol{\delta}_2-\boldsymbol{k}\boldsymbol{\delta}_1-\hat{\boldsymbol{W}}^{\mathrm{T}}\boldsymbol{h}+\boldsymbol{x}_{\mathrm{pld}}'+\boldsymbol{W}^{*\mathrm{T}}\boldsymbol{h}+\boldsymbol{\varepsilon}_{\mathrm{n}}-\boldsymbol{x}_{\mathrm{pld}}'\right)+$$
$$\sum_{i=x}^{z}\Gamma_i^{-1}\tilde{\boldsymbol{W}}_i^{\mathrm{T}}\hat{\boldsymbol{W}}_i'=\boldsymbol{\delta}_1^{\mathrm{T}}\left(\boldsymbol{\delta}_2-\boldsymbol{k}\boldsymbol{\delta}_1-\tilde{\boldsymbol{W}}^{\mathrm{T}}\boldsymbol{h}+\boldsymbol{\varepsilon}_{\mathrm{n}}\right)+\sum_{i=x}^{z}\Gamma_i^{-1}\tilde{\boldsymbol{W}}_i^{\mathrm{T}}\hat{\boldsymbol{W}}_i' \tag{35}$$

Expanding Eq.(35) leads to

$$V_2'=\boldsymbol{\delta}_1^{\mathrm{T}}\boldsymbol{\delta}_2-\boldsymbol{\delta}_1^{\mathrm{T}}\boldsymbol{k}\boldsymbol{\delta}_1+\boldsymbol{\delta}_1^{\mathrm{T}}\boldsymbol{\varepsilon}_{\mathrm{n}}+\sum_{i=x}^{z}\Gamma_i^{-1}\tilde{\boldsymbol{W}}_i^{\mathrm{T}}\left(-\Gamma_i\delta_{1i}\boldsymbol{h}_i+\hat{\boldsymbol{W}}_i'\right) \tag{36}$$

Substituting the adaptive law described in Eq.(16) into Eq.(36) leads to

$$V_2'=\boldsymbol{\delta}_1^{\mathrm{T}}\boldsymbol{\delta}_2-\boldsymbol{\delta}_1^{\mathrm{T}}\boldsymbol{k}\boldsymbol{\delta}_1+\boldsymbol{\delta}_1^{\mathrm{T}}\boldsymbol{\varepsilon}_{\mathrm{n}}-\sum_{i=x}^{z}\sigma_i\Gamma_i^{-1}\tilde{\boldsymbol{W}}_i^{\mathrm{T}}\hat{\boldsymbol{W}}_i=$$
$$\sum_{i=x}^{z}\delta_{1i}\delta_{2i}-k_i\delta_{1i}\delta_{1i}+\delta_{1i}\varepsilon_{in}-\sigma_i\Gamma_i^{-1}\tilde{\boldsymbol{W}}_i^{\mathrm{T}}\hat{\boldsymbol{W}}_i \tag{37}$$

With $2ab\leqslant a^2+b^2$, the following inequality holds

$$\delta_{1i}\varepsilon_{in}\leqslant\frac{1}{4}\delta_{1i}\delta_{1i}+\varepsilon_{in}^2$$

Based on $|\varepsilon_{in}|\leqslant\bar{\varepsilon}_{\mathrm{n}}(i=x,y,z)$, inequality turns into

$$\delta_{1i}\varepsilon_{in}\leqslant\frac{1}{4}\delta_{1i}\delta_{1i}+\bar{\varepsilon}_{\mathrm{n}}^2$$

It is proved that $\boldsymbol{\delta}_2$ converges within a finite time in subsection (1), Eq.(37) turns into

$$V_2'\leqslant\sum_{i=x}^{z}\left(-k_i+\frac{1}{4}\right)\delta_{1i}\delta_{1i}+\bar{\varepsilon}_{\mathrm{n}}^2-\sigma_i\Gamma_i^{-1}\tilde{\boldsymbol{W}}_i^{\mathrm{T}}\hat{\boldsymbol{W}}_i \tag{38}$$

According to Eq.(14), Eq.(38) turns into

$$V_2'\leqslant\sum_{i=x}^{z}\left(-k_i+\frac{1}{4}\right)\delta_{1i}\delta_{1i}+\bar{\varepsilon}_{\mathrm{n}}^2-\frac{\sigma_i}{2}\Gamma_i^{-1}\tilde{\boldsymbol{W}}_i^{\mathrm{T}}\tilde{\boldsymbol{W}}_i \tag{39}$$

Eq.(39) can be rewritten as

$$V_2'\leqslant-\mu V_2+\eta \tag{40}$$

where $\eta=3\bar{\varepsilon}_{\mathrm{n}}^2$ is a positive constant, and

$$\mu=\min_{i=x,y,z}2\left\{k_i-\frac{1}{4},\frac{\sigma_i}{2}\right\}$$

As long as parameters $\boldsymbol{k}$ and $\boldsymbol{\sigma}$ are designed properly, $\mu>0$ can be satisfied, and a conclusion can be drawn that the relative position error $\boldsymbol{\delta}_1$ is stable.

Furthermore, multiplying both sides of Eq.(40) by $e^{\mu\theta}$ leads to

$$\frac{\mathrm{d}}{\mathrm{d}\theta}\left(V_2e^{\mu\theta}\right)\leqslant e^{\mu\theta}\eta \tag{41}$$

Integrating Eq.(41) leads to

$$V_2\leqslant\frac{\eta}{\mu}+\left[V_2(0)-\frac{\eta}{\mu}\right]e^{-\mu\theta}\leqslant\frac{\eta}{\mu}+V_2(0) \tag{42}$$

According to Eq.(31), there is

$$\|\boldsymbol{\delta}_1\|^2\leqslant2\left[V_2(0)-\frac{\eta}{\mu}\right]e^{-\mu\theta}+\frac{2\eta}{\mu}$$
$$\sum_{i=x}^{z}\|\tilde{\boldsymbol{W}}_i\|^2\leqslant2\min_{i=x,y,z}(\Gamma_i)\left(\left[V_2(0)-\frac{\eta}{\mu}\right]e^{-\mu\theta}+\frac{\eta}{\mu}\right)$$

For $\forall\theta\geqslant0$, the following result can be obtained

$$\lim_{\theta\to\infty}\|\boldsymbol{\delta}_1\|=\sqrt{2\eta/\mu}$$
$$\lim_{\theta\to\infty}\sum_{i=x}^{z}\|\tilde{\boldsymbol{W}}_i\|=\sqrt{2\min_{i=x,y,z}(\Gamma_i)\eta/\mu}$$

Then the Lyapunov function described in Eq.(31) can be written as

$$V_2=\boldsymbol{E}^{\mathrm{T}}(\theta)\boldsymbol{\Sigma}^{-1}\boldsymbol{E}(\theta)/2$$

where

$$\boldsymbol{E}(\theta)=\left[\tilde{\boldsymbol{W}}_x,\tilde{\boldsymbol{W}}_y,\tilde{\boldsymbol{W}}_z,\boldsymbol{\delta}_1\right]^{\mathrm{T}}$$
$$\boldsymbol{\Sigma}=\mathrm{diag}\left\{\mathrm{diag}\left\{\Gamma_i\right\},1\right\}$$

There holds the following inequality

$$2\lambda_{\min}(\boldsymbol{\Sigma})\|\boldsymbol{E}(\theta)\|^2\leqslant V_2\leqslant2\lambda_{\max}(\boldsymbol{\Sigma})\|\boldsymbol{E}(\theta)\|^2 \tag{43}$$

According to Eq.(42), Eq.(43) can be transformed into

$$a\leqslant V_2\leqslant p$$

where

$$a=\left[3+\lambda_{\min}(\Gamma_i)\right]\eta/\mu$$

and a compact set is defined as

$$\Xi=\left\{a\leqslant p\text{ and }2\lambda_{\min}(\boldsymbol{\Sigma})\|\boldsymbol{E}(\theta)\|^2<p\right\}$$

According to Lemma 2 (see the Appendix), the relative position error $\boldsymbol{\delta}_1$ and estimate weight error vector $\tilde{\boldsymbol{W}}$ are bounded in finite time.

(3) Finiteness of convergence time of $\boldsymbol{\delta}_2$

There are two convergence processes. Suppose that the system state reaches the sliding mode surface at a time θ_1. Afterwards, $\boldsymbol{\delta}_2$ and $\boldsymbol{\delta}_2'$ converge at a time θ_2. Then the convergence time of the system is $\theta_s=\theta_1+\theta_2$.

When the sliding mode surface converges to zero, i.e. $\boldsymbol{s}=\boldsymbol{\delta}_2+\beta\boldsymbol{\delta}_2'^{\gamma}=0$, then

$$\boldsymbol{\delta}_2'=-\beta^{-\frac{1}{\gamma}}\boldsymbol{\delta}_2^{\frac{1}{\gamma}} \tag{44}$$

Define a Lyapunov function as

$$V_3=\frac{1}{2}\boldsymbol{\delta}_2^{\mathrm{T}}\boldsymbol{\delta}_2 \tag{45}$$

Taking derivative of Eq.(45) leads to

$$V_3'=\boldsymbol{\delta}_2^{\mathrm{T}}\boldsymbol{\delta}_2' \tag{46}$$

Substitute Eq.(44) into Eq.(46) and rewrite Eq.(46) in the form of addition of triaxial components

$$\begin{aligned}V_3'=&\sum_{i=x}^{z}\delta_{2i}\delta_{2i}'=\\&-\sum_{i=x}^{z}\delta_{2i}\beta^{-\frac{1}{\gamma}}\delta_{2i}^{\frac{1}{\gamma}}=\\&-\sum_{i=x}^{z}\beta^{-\frac{1}{\gamma}}\delta_{2i}^{1+\frac{1}{\gamma}}\end{aligned} \tag{47}$$

Eq.(47) can also be rewritten as

$$V_3'=-\sum_{i=x}^{z}\beta_i^{-\frac{1}{\gamma}}\delta_{2i}^{\frac{1}{\gamma}+1}\leqslant-\alpha V_3^{p}$$

where $\alpha=\min\beta_i^{-1/\gamma}$, $p=(1+\gamma)/2\gamma$.

According to Lemma 3 (see the Appendix), the settling time of each axis can be expressed as

$$\theta_{2i}=\beta^{\gamma}\frac{\gamma}{\gamma-1}\left|\delta_{2i}(t_1)\right|^{(\gamma-1)/\gamma}$$

where $i=x,y,z$. Then $\theta_2\leqslant\max\limits_{i=x,y,z}\theta_{2i}$. The relative speed error $\boldsymbol{\delta}_2$ converges within finite time $\theta_s=\theta_1+\theta_2$.

4 Simulation

In this section, to validate that the control scheme designed is effective, the application of the proposed control scheme to a satellite rendezvous is demonstrated[35].

The AOE of the leader satellite is shown in Table 1. Suppose a satellite weighting 50 kg can provide maximum output of 2 N using a chemical acceleration module, and is equipped with electric propulsion offering a thrust of 10—100 mN[38-40]. Suppose the initial relative position of two satellites is $\boldsymbol{x}_{\mathrm{p1}}(\theta_0)=[-800\quad 600\quad 500]^{\mathrm{T}}$ m, the initial relative velocity is $\boldsymbol{x}_{\mathrm{p2}}(\theta_0)=[2\quad 3\quad 2]^{\mathrm{T}}$ m/s. The expected relative position of two satellites is $\boldsymbol{x}_{\mathrm{p1d}}=[-20\quad 20\quad 20]^{\mathrm{T}}$ m, and the expected relative velocity is $\boldsymbol{x}_{\mathrm{p2d}}=[0\quad 0\quad 0]^{\mathrm{T}}$ m/s.

The satellite orbit is affected by various perturbations and disturbances in outer space, leading to model uncertainties. Major perturbations include nonspherical perturbations, the third body attraction perturbations, sunlight pressure perturbations and so on. The numerical values of these perturbations are small compared to Earth gravity. Nevertheless, their long term influences cannot be ignored.

Table 1 Initial orbit elements of the leader satellite

a/km	e	i/(°)	Ω/(°)	w/(°)	M/(°)
10 000	0.2	20	60	0	0

$\Delta\boldsymbol{A}$ presents model uncertainties, which are related to system states and true anomaly, and the external disturbances $\boldsymbol{d}$ are only related to true anomaly. $\Delta\boldsymbol{A}$ and $\boldsymbol{d}$ are considered as

$$\Delta\boldsymbol{A}=0.1\times\begin{bmatrix}x\cos\left(\frac{\pi}{20}\theta-0.1\right)\\-y\sin\left(\frac{\pi}{50}\theta\right)\\-z\sin\left(\frac{\pi}{30}\theta+0.1\right)\end{bmatrix}$$

$$\boldsymbol{d}=0.1\times\begin{bmatrix}5+3.5\sin\left(\frac{\pi}{100}\theta\right)-1.5\tanh\left(\frac{\pi}{100}\theta\right)\\4-2.5\sin\left(\frac{\pi}{100}\theta\right)+\tanh\left(\frac{\pi}{100}\theta\right)\\-5+2.5\sin\left(\frac{\pi}{100}\theta\right)+0.5\tanh\left(\frac{\pi}{100}\theta\right)\end{bmatrix}$$

(1) Case 1: Repetitive control scheme without disturbances

By implanting a dynamic model of the tracking signal into the controller, the repetitive controller can track any periodic signal with no steady state error. An ideal situation is set, where no disturbances exist, and the position tracking ability of repetitive control is analyzed. Fig.5 shows the position tracking results by the repetitive controller. Fig.5 indicates that repetitive control can make position states track the expected signals precisely after the true anomaly of 10 rad.

The steady state error is illustrated in Fig.6. It can be observed that the position tracking error e is bounded and converges to zero domain. The precision of relative position tracking is within 2 m.

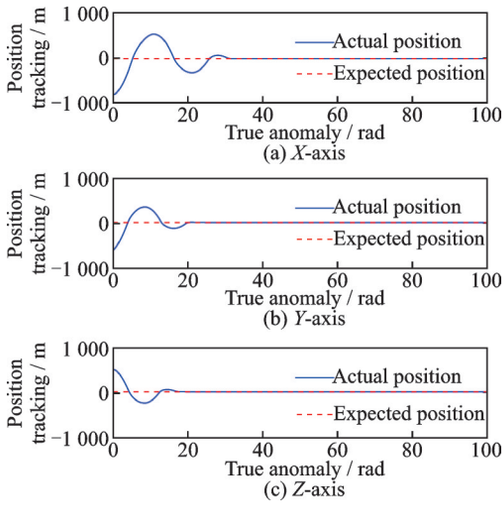

Fig.5 Position tracking by repetitive controller

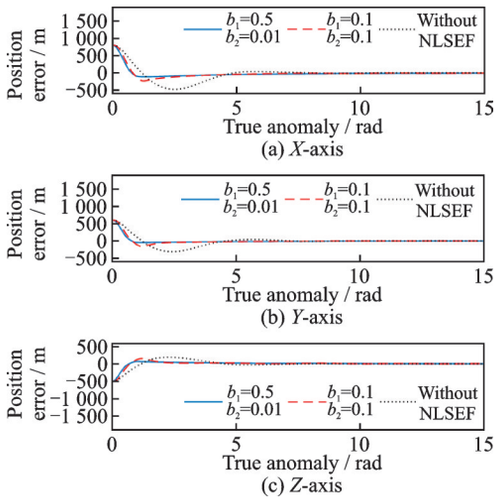

Fig.7 Regulating process by NLSEF

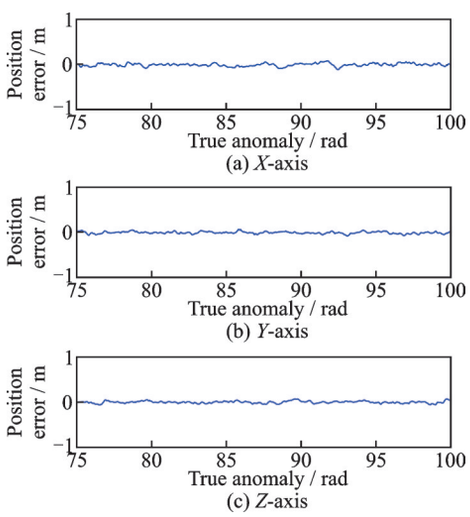

Fig.6 Relative position error by repetitive controller

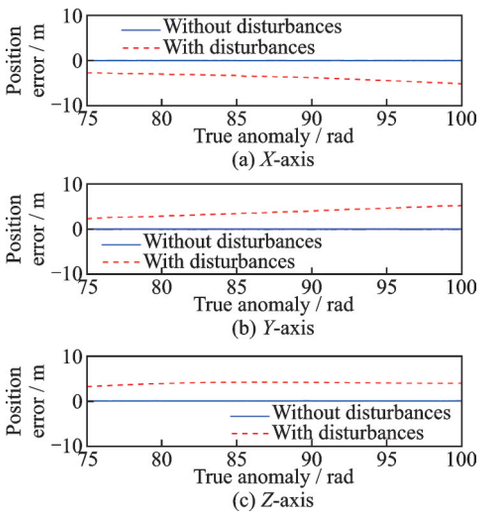

Fig.8 Precision comparison in two situations

NLSEF is able to improve the dynamic performance of the repetitive controller. Parameters b_1 and b_2 of NLSEF control law $\boldsymbol{u}_0$ contribut the most to the regulating process. It can be observed from Fig.7 that the NLSEF helps repetitive controller gain less overshoot and faster respond speed.

(2)Case 2: Repetitive control scheme with disturbances

In reality, various disturbances in outer space are inevitable. In this case, the model uncertainties $\Delta \boldsymbol{A}$ and unknown disturbances $\boldsymbol{d}$ are considered in the simulation, and the system is still controlled by a repetitive control scheme only. In Fig.8, the position tracking errors are demonstrated and compared with that in Case 1.

From Fig.8, it is obvious that if the system is controlled by the repetitive control scheme only, the position tracking errors tend to diverge with the impact of disturbances. The results prove that the repetitive control does little work dealing with the disturbances, and improvement is necessary for satellite rendezvous.

(3)Case 3: IRC scheme with disturbances

Given unknown disturbances and model uncertainties, the response curves of the relative position maintained by the IRC scheme designed in our study are shown in Fig.9, and the response curves of the relative velocity are shown in Fig.10.

In Figs.9, 10, relative position and velocity response curves converge after 5 rad. The results prove that the controller is stable and convergent despite the disturbances.

Note that the velocities peak at first 0.05 rad. According to Fig.11, the maximum control forces

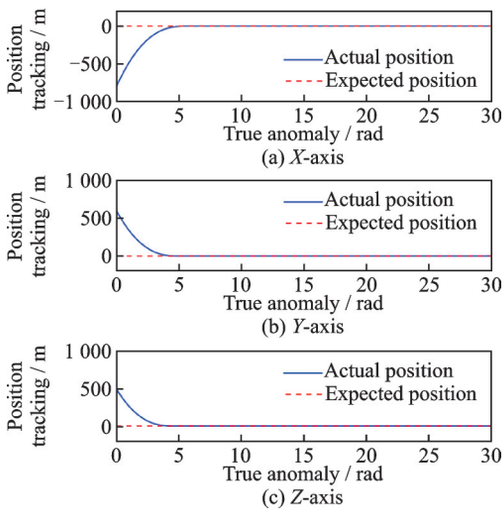

Fig.9 Position tracking by IRC

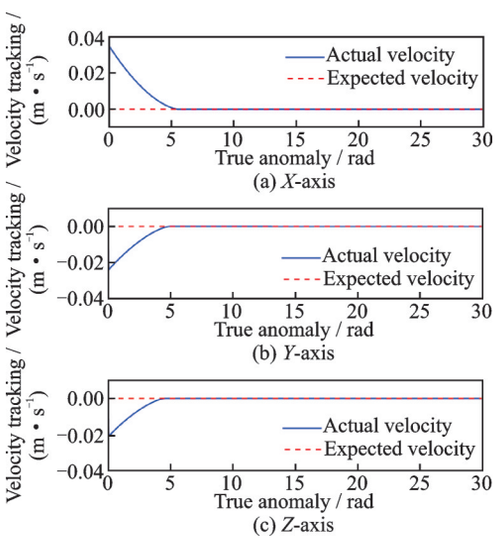

Fig.10 Velocity tracking by IRC

needed are less than 2 N and meet the requirement.

Figs.12, 13 demonstrate the performance of the IRC scheme at a steady state, emphasizing the period of 16 rad to 25 rad, where the follower satellite keeps hovering against the leader satellite.

When the satellites come to a steady state, the precision of the relative position is better than 5×10^{-4} m, and the control force is less than 100 mN. The accuracy achieves millimeter level, and the maintenance forces can be afforded by an electric propulsion[39]. Moreover, the output curves are quite smooth without obvious buffeting.

To demonstrate the advantages of the IRC scheme, the contribution of the repetitive controller is eliminated in Fig.14.

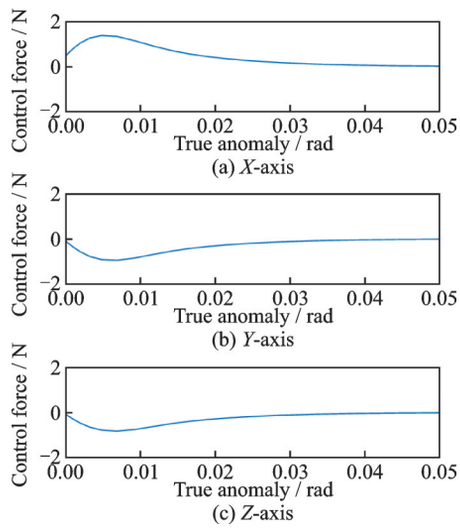

Fig.11 Control variable by IRC in transferring state

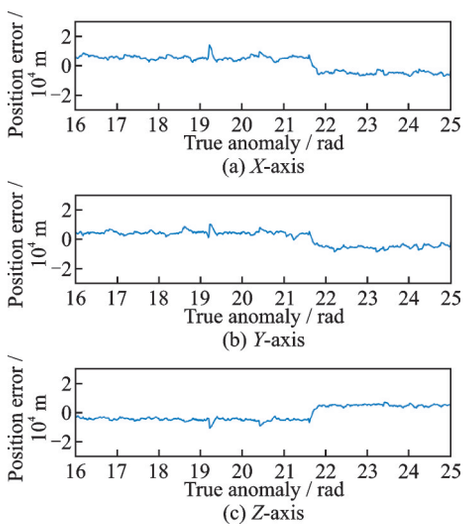

Fig.12 Relative position error by IRC

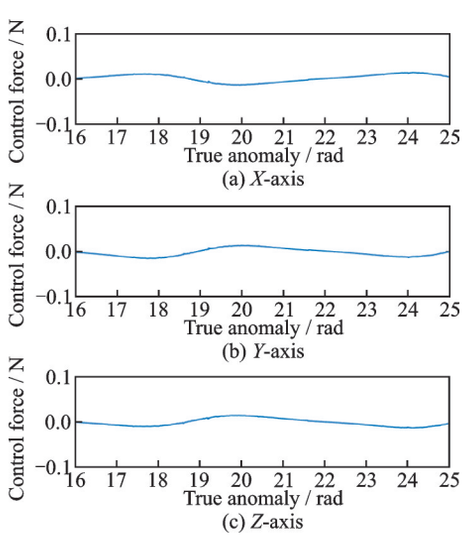

Fig.13 Control variable by IRC in steady state

Apparently, the precision of the system deteriorates when the contribution of the repetitive con-

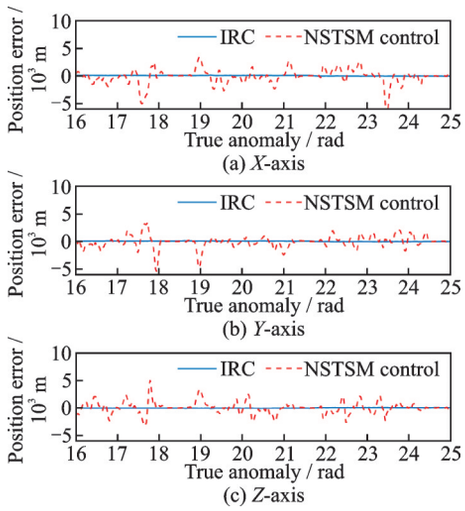

Fig.14 Precision comparison between two control schemes

troller is eliminated. The results prove that the IRC scheme improves the accuracy of the sliding mode controller by more than one order of magnitude.

Further, to demonstrate that the IRC scheme designed in this paper has the advantage of converging in finite time, a comparative simulation is shown in Fig.15, comparing IRC with the traditional backstepping control scheme.

As analyzed in Section 3, and according to Lemma 3, the IRC ensures that after the system states reach the sliding mode surface, the relative position error $\boldsymbol{\delta}_1$ converges to a small neighborhood of the origin $\left[-\sqrt{2\eta/\mu}, \sqrt{2\eta/\mu}\right]$ within finite time $\theta_{2i}=\beta^{\gamma}\cdot\gamma/(\gamma-1)\cdot\left|\delta_{2i}(t_1)\right|^{(\gamma-1)/\gamma}$.

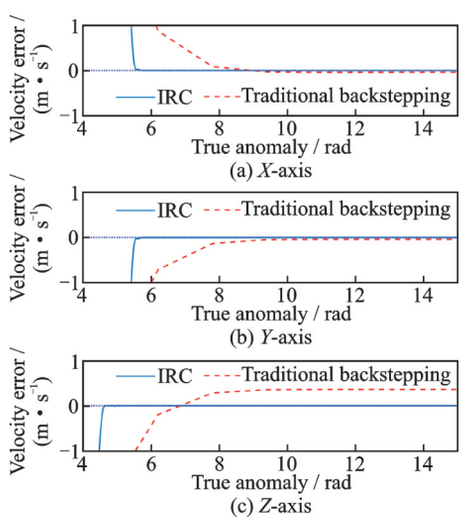

Fig.15 Convergence comparison between two control schemes

In Case 3, we can find in Fig.15 that IRC makes the system states reach the neighborhood $[-0.077, 0.077]$ m within $\theta_s=5.23$ rad, while the traditional backstepping control is unable to converge to neighborhood in time.

Fig.15 proves that the IRC converges in finite time. Nevertheless, the rapidity of the IRC is not satisfying, and worth further investigation.

5 Conclusions

Our study aims at high-precision satellite rendezvous control, and proposes an improved repetitive control (IRC) scheme. The controlled model described by ROE in the form of state space equations has both advantages of high accuracy and great adaptability. The repetitive controller makes the follower satellite track the expected signals precisely, while the siding mode controller solves the divergence problem caused by the aperiodic disturbances and makes the repetitive controller robust. Moreover, NLSEF is effective to improve the dynamic performance of the controller.

The rapidity of the controller is not studied in this paper, and could be further improved in future work. Also, it is worth considering the situation when the rendezvous object is uncooperative in the future.

Appendix

Lemmal 1[41] Consider a dynamic system

$$\begin{cases}\dot{x}_1=x_2\\ \dot{x}_2=f(x_1,x_2)+u\\ y=x_1\end{cases}\tag{A1}$$

An extended state observer is constructed instead of identifying the unknown function $f(x_1,x_2)$ in the system

$$\begin{cases}\dot{z}_1=z_2-g_1(y-z_1)\\ \dot{z}_2=a+u-g_2(y-z_1)\\ \dot{a}=-g_3(y-z_1)\end{cases}\tag{A2}$$

The state variables of the observer z_1 and z_2 track the state variables of the system described in Eq.(A1) x_1 and x_2. Especially, $a(t)$ estimates $f(x_1,x_2)$ in real time.

Lemma 2[42] Let $D\subset\mathbf{R}^n$ denote a domain containing the origin, there is a continuously differentiable and positive

definite function $L(t,x)\in[0,\infty)\times D$, which satisfies the following conditions

$$W_1(x)\leqslant L(t,x)\leqslant W_2(x)$$

$$\dot{L}(t,x)\leqslant -\mu W_3(x)+\phi$$

where ϕ is a positive real number; and for $\forall t\geqslant 0$, $\forall x\in D$, it is promised that $W_1(x)$, $W_2(x)$ and $W_3(x)$ are all continuous and positive definite functions on D, and there is a positive constant c, so that $\Xi=\{W_1(x)\leqslant c \text{ and } W_2(x)<c\}$ is a compact subset of D. Then the function $L(t,x)$ is able to converge within a bounded compact set in finite time.

Lemma 3[43] Consider a system of differential equations

$$\dot{x}=f(\boldsymbol{x}(t)),\ \boldsymbol{x}(0)=x_0 \tag{A3}$$

where $\boldsymbol{x}=[x_1,x_2,\cdots,x_n]^{\mathrm{T}}\in\mathbf{R}^n$, $f(x):\mathbf{R}^n\to\mathbf{R}^n$ is continuous on $\mathbf{R}^n$ and $f(0)=0$.

For the system described in Eq.(A2), if there exists a continuous positive definite function $V(\boldsymbol{x}):\mathbf{R}^n\to\mathbf{R}$, and so does the continuous first-order partial derivative with respect to any x, such that there exist real numbers α and $p\in(0,1)$, and they satisfy that

$$\dot{V}(\boldsymbol{x})+\alpha(V(\boldsymbol{x}))^p\leqslant 0,\ \boldsymbol{x}\in\mathbf{R}^n\backslash\{0\}$$

Then the origin is a globally finite time stable equilibrium of Eq.(A2). That means the system can converge to the neighborhood of designate point within time T. The upper bound of the settling time is

$$T(x_0)\leqslant\frac{1}{\alpha(1-p)}V(x_0)^{(1-p)}$$

References

[1] CLOHESSY W H, WILTSHIRE R S. Terminal guidance system for satellite rendezvous[J]. Journal of the Aerospace Sciences, 1960, 27(9): 653-658.

[2] BAINUM P M. Breakwell memorial lecture: Review of astrodynamics 1958—2001, a personal perspective[J]. Acta Astronautica, 2002, 51: 517-526.

[3] HILL G W. Researches in the lunar theory[J]. American Journal of Mathematics, 1878, 1(2): 5-26.

[4] LONDON H S. Second approximation to the solution of the rendezvous equations[J]. AIAA Journal, 1963, 1: 1691-1693.

[5] YAMANAKA K, ANKERSEN F. New state transition matrix for relative motion on an arbitrary elliptical orbit[J]. Journal of Guidance Control and Dynamics, 2002, 25(1): 60-66.

[6] OGUNDELE A D. Modeling and analysis of nonlinear spacecraft relative motion via harmonic balance and Lyapunov function[J]. Aerospace Science and Technology, 2020, 99: 105761.

[7] SABOL C, BURNS R, MCLAUGHLIN C A. Formation flying design and evolution[J]. Journal of Spacecraft and Rockets, 2001, 38(2): 270-278.

[8] SCHWEIGHART S, SEDWICK R. High-fidelity linearized J2 model for satellite formation flight[J]. Journal of Guidance, Control and Dynamics, 2004, 25(6): 1073-1080.

[9] TSCHAUNER J, HEMPEL P. Rendezvous zu einem in elliptischer bahn umlaufenden ziel[J]. Acta Astronautica, 1965, 2: 104-109.

[10] INALHAN G, TILLERSON M, HOW J P. Relative dynamics and control of spacecraft formations in eccentric orbits[J]. Journal of Guidance, Control and Dynamics, 2002, 25(1): 48-60.

[11] SCHAUB H. Relative orbit geometry through classical orbit element differences[J]. Journal of Guidance Control and Dynamics, 2004, 27(5): 839-848.

[12] OGUNDELE A D. Approximate analytic solution of nonlinear Riccati spacecraft formation flying dynamics in terms of orbit element differences[J]. Aerospace Science and Technology, 2021, 113: 106686.

[13] RAO Y, YIN J, HAN C. Hovering formation design and control based on relative orbit elements[J]. Journal of Guidance Control and Dynamics, 2015, 152(2): 1-12.

[14] BAI S Z, CHAO H, SUN X C, et al. Teardrop hovering formation for elliptical orbit considering J2 perturbation[J]. Aerospace Science and Technology, 2020, 106: 106098.

[15] SANCHEZ J C, LOUEMBET C, GAVILAN F, et al. An event-triggered predictive controller for spacecraft rendezvous hovering phases[J]. IFAC-Papers Online, 2019, 52(12): 97-102.

[16] AKIYAMA Y, BANDO M, HOKAMOTO S. Station-keeping and formation flying based on nonlinear output regulation theory[J]. Acta Astronautica, 2018, 153: 289-296.

[17] ZHOU Y, YAN Y, HUANG X, et al. Multi-objective and reliable output feedback control for spacecraft hovering[J]. Journal of Aerospace Engineering, 2015, 229(10): 1798-1812.

[18] D'AMICO S. Autonomous formation flying in low earth orbit[D]. The Netherland: Technical University of Delft, 2010.

[19] ZHENG D, LUO J, YIN Z, et al. Finite-time velocity-free prescribed performance control for Halo orbit autonomous rendezvous[J]. Journal of Aerospace En-

gineering, 2021, 235(2): 205-218.

[20] SU P, FENG W, KUN Y, et al. Optimal control of rapid cooperative spacecraft rendezvous with multiple specific-direction thrusts[J]. Journal of Aerospace Engineering, 2020, 234(16): 2296-2322.

[21] ROUZEGAR H, KHOSRAVI A, SARHADI P. Spacecraft formation flying control under orbital perturbations by state-dependent Riccati equation method in the presence of on-off actuators[J]. Journal of Aerospace Engineering, 2019, 233(8): 2853-2867.

[22] WU G, SONG S M, SUN J. Finite-time antisaturation control for spacecraft rendezvous and docking with safe constraint[J]. Journal of Aerospace Engineering, 2019, 233(6): 2170-2184.

[23] ZHANG L, GE P Q. High precision dynamic model and control considering J2 perturbation for spacecraft hovering in low orbit[J]. Advances in Space Research, 2021, 67(7): 2185-2198.

[24] HUANG X, YAN Y, ZHOU Y, et al. Sliding mode control for Lorentz-augmented spacecraft hovering around elliptic orbits[J]. Acta Astronautica, 2014, 103: 257-268.

[25] ZHOU Y, YAN Y, HUANG X. Multi-objective robust controller design for spacecraft hovering around elliptical orbital target[J]. Journal of Systems and Control Engineering, 2015, 229(4): 356-371.

[26] NAMDARI H, ALLAHVERDIZADEH F, SHARIFI A. Robust composite nonlinear feedback control for spacecraft rendezvous systems under parameter uncertainty, external disturbance, and input saturation[J]. Journal of Aerospace Engineering, 2020, 234(2): 143-155.

[27] LIU J, LI H, LUO Y, et al. Robust adaptive relative position and attitude integrated control for approaching uncontrolled tumbling spacecraft[J]. Journal of Aerospace Engineering, 2020, 234(2): 361-374.

[28] IMANI A, BEIGZADEH B. Robust control of spacecraft rendezvous on elliptical orbits: Optimal sliding mode and backstepping sliding mode approaches[J]. Journal of Aerospace Engineering, 2016, 230(10): 1975-1989.

[29] HE S, WANG W, LIN D, et al. Robust output feedback control design for autonomous spacecraft rendezvous with actuator faults[J]. Journal of Systems and Control Engineering, 2016, 230(6): 578-587.

[30] LI C Y, ZHOU L. Design of robust sliding mode variable structure repetitive control system[J]. Control Engineering of China, 2018, 164(8): 119-124.

[31] HAN C, YIN J F. Study of satellite relative motion in elliptical orbit using relative orbit elements[J]. Chinese Journal of Aeronautics, 2011, 32(12): 2244-2258.

[32] DANG Z H. New state transition matrix for relative motion on an arbitrary keplerian orbit[J]. Journal of Guidance Control and Dynamics, 2017, 40(11): 2917-2927.

[33] HAN J Q, WANG W. A new type of controller: NLPID[J]. Control and Decision, 1994, 9(6): 401-407.

[34] CHEN S Y, LIN F J. Robust nonsingular terminal sliding-mode control for nonlinear magnetic bearing system[J]. IEEE Transactions on Control Systems Technology, 2011, 19(3): 636-643.

[35] ZHANG K, DUAN G R. Fast finite-time tracking control for the mechanical system and its application to spacecraft rendezvous system[J]. Control Theory and Applications, 2019, 36(1): 87-95.

[36] ZUO Z. Non-singular fixed-time terminal sliding mode control of non-linear systems[J]. IET Control Theory and Applications, 2014, 9(4): 545-552.

[37] WANG J H, HU J B. Adaptive backstepping high-order terminal sliding mode control for uncertain nonlinear systems[J]. Control and Decision, 2012, 27(3): 413-418.

[38] LIU R X, CAO X B, LIU M. Finite-time synchronization control of spacecraft autonomous rendezvous with elliptical orbits and thrust faults[J]. IEEE Access, 2017, 5: 24853-24862.

[39] BAKER A M, CURIEL A D S, SCHAFFNER J, et al. "You can get there from here": Advanced low cost propulsion concepts for small satellites beyond LEO [J]. Acta Astronautica, 2005, 57: 288-301.

[40] SALMIN V V, PETRUKHINA K V, KVETKIN A A. Transfer of a satellite from high elliptical to geostationary orbit with the help of electric propulsion[J]. Procedia Engineering, 2017, 185: 352-358.

[41] HAN J Q. The "extended state observer" of a class of uncertain systems[J]. Control and Decision, 1995, 10(1): 85-88.

[42] VIJAY M, JENA D. Backstepping terminal sliding mode control of robot manipulator using radial basis functional neural networks[J]. Computers and Electrical Engineering, 2018, 67: 690-707.

[43] ZUO Z, TIE L. A new class of finite-time nonlinear consensus protocols for multi-agent systems[J]. Inter-

national Journal of Control, 2014, 87(2): 363-37.

Acknowledgements This work was supported by the National Natural Science Foundation of China (No.61873127) and the Key International (Regional) Cooperative Research Projects of the National Natural Science Foundation of China (No.62020106003).

Authors Ms. **ZHANG Yi** received the B.S. degree in detection, guidance and control techniques from Nanjing University of Aeronautics and Astronautics (NUAA), Nanjing, China, in 2019. She is currently pursuing the M.S. degree at the College of Automation, NUAA, Nanjing, China. Her current research interests include satellite rendezvous control, sliding mode control, and neural adaptive control.

Prof. **QI Ruiyun** received the B.S. degree in automatic control from University of Science and Technology of China, Hefei, China, in 2001, and the Ph.D. degree in electronics, electrical and computer engineering from University of Birmingham, Birmingham, UK, in 2007. From 2008 to present, she has been with the College of Automation, NUAA, where she is currently a full professor. Her research has focused on fuzzy adaptive control, fault-tolerant control and their applications.

Author contributions Ms. **ZHANG Yi** contributed to the discussion and background, designed the controller, conducted the analysis and wrote the manuscript. Prof. **QI Ruiyun** designed the study. All authors commented on the manuscript and approved the submission.

Competing interests The authors declare no competing interests.

(Production Editor: ZHANG Bei)

航天器高精度悬停的改进型重复控制

张 翼, 齐瑞云

(南京航空航天大学自动化学院,南京 211106, 中国)

摘要:研究了以高精度为目的的航天器悬停系统控制设计。采用相对轨道要素描述目标航天器和跟踪航天器之间的相对运动模型,具有清晰的几何意义和较高的精度。为了实现高精度的相对位置和相对速度跟踪,提出了一种改进型重复控制方案,该方案利用重复控制能够精确跟踪目标信号的优点,并通过加入非奇异终端滑模控制器克服了传统重复控制器易受非周期干扰影响的缺点。此外,利用非线性状态误差反馈改善了重复控制器的动态性能,并利用径向基函数神经网络逼近悬停模型的未知非线性项。通过严格的李雅普诺夫稳定性分析,保证了整个闭环控制系统的稳定性。最后,通过数值仿真验证了所提控制方案的有效性和优越性。

关键词:航天器悬停;相对轨道要素;重复控制;滑模控制;径向基函数神经网络